J Inorg Organomet Polym (2013) 23:1485–1491
DOI 10.1007/s10904-013-9953-3

# Polyaniline/Montmorillonite Nanocomposites Obtained by In Situ Intercalation and Oxidative Polymerization in Cationic Modified-Clay (Sodium, Copper and Iron)

**A. Zehhaf · E. Morallon · A. Benyoucef**

Received: 4 May 2013 / Accepted: 26 August 2013 / Published online: 11 September 2013


**Abstract** Polyaniline/montmorillonite nanocomposites (PANI/M) were obtained by intercalation of aniline monomer into M modified with different cations and subsequent oxidative polymerization of the aniline. The modified-clay was prepared by ion exchange of sodium, copper and iron cations in the clay (Na–M, Cu–M and Fe–M respectively). Infrared spectroscopy confirms the electrostatic interaction between the oxidized PANI and the negatively charged surface of the clay. X-ray diffraction analysis provides structural information of the prepared materials. The nanocomposites were characterized by transmission electron microscopy and their thermal degradation was investigated by thermogravimetric analysis. The weight loss suggests that the PANI chains in the nanocomposites have higher thermal stability than pure PANI. The electrical conductivity of the nanocomposites increased between 12 and 24 times with respect to the pure M and this increase was dependent on the cation-modification. The electrochemical behavior of the polymers extracted from the nanocomposites was studied by cyclic voltammetry and a good electrochemical response was observed.

**Keywords** Oxidative polymerization · Polyaniline · Nanocomposite · Conducting polymer · Montmorillonite · Cation-exchanged

A. Zehhaf · A. Benyoucef (✉)
Laboratoire de Chimie Organique, Macromoléculaire et des Matériaux, Université de Mascara, Bp 763, 29000 Mascara, Algeria
e-mail: ghani29000@yahoo.fr

E. Morallon
Departamento de Química Física and Instituto Universitario de Materiales, Universidad de Alicante, Apartado 99, 03080 Alicante, Spain

## 1 Introduction

During the last years, academic and industrial communities have dedicated intense efforts in the development of polymer/clay nanocomposite (PCN) materials. These materials usually demonstrate properties superior to conventional ones. In general, they combine both the characteristics of the inorganic template and the organic polymers at the molecular level [1]. Currently, the PCN material is found to be a promising system because the clay possesses a high aspect ratio and a platy morphology. It can be employed to boost the physical properties of bulk polymers being the mechanical properties a significant issue for application and development of these materials. Kim and White [2] reported a variety of organic modified montmorillonites to understand the contribution of the organophilicity of organoclay on the formation of the PCN [3–5].

The significance of the organoclay is that even less than 5 wt% of clay loading in any reinforcing component could improve hundreds of engineering properties which include fire retardancy [6–8], barrier resistance [9, 10], and ionic conductivity [11, 12]. It is clear from this evidence that PCNs are good demonstration of nanotechnology. Another interest in developing PCNs is that they can be applied immediately in commercial applications [13].

Polymer clay nanocomposites based on polyaniline/montmorillonite (PANI/M) are obtained by the polymerization of anilinium ions within the interlayer space of M [14, 15]. The electrically conducting polymers incorporated into clay have attracted great attention due to their potential technological applications in light-emitting diodes, lightweight battery electrodes, sensors, electro-optics, electromagnetic shielding materials, fuel cell electrodes and as anticorrosive coatings [16–18]. Among the conducting polymers, PANI is a promising polymer due to

its simple synthesis, high electrical conductivity and excellent chemical stability [19]. However, its poor thermal and mechanical properties restrict its commercial applications and, therefore, methods to improve such properties are of great importance [20]. PANI/clay nanocomposites have numerous potential applications including electrodes for rechargeable batteries [21], electrodes for energy storage devices [22], electromagnetic interference shielding [23], electronic and optical devices [24], smart windows [22] and in light emitting diodes [22, 25].

Montmorillonite is constituted by two dimensional silicate anions with cations between the layers that can be easily exchanged. Thus, the interlayer spacing can be modified, depending on the cation intercalated. Therefore, the use of modified montmorillonite with different inorganic cations can affect properties like electrical conductivity of PCN. For this reason, in this work, the synthesis of nanocomposites of PANI with a natural montmorillonite modified with inorganic cations ($Na^+$, $Cu^{2+}$ and $Fe^{2+}$) is reported. The PANI/clay nanocomposites were prepared by introducing the aniline monomer into the clay galleries containing $Na^+$, $Cu^{2+}$, $Fe^{2+}$ (by cation exchange) and allowing to polymerize to form extended chains of PANI in the montmorillonite interlayers. The characterization of the PANI/clay nanocomposites by X-ray diffraction (XRD), transmission electron microscopy (TEM), Fourier transform Infrared spectroscopy (FTIR), thermogravimetric analysis (TGA) and cyclic voltammetry, is also performed.

## 2 Experimental

### 2.1 Materials

Aniline (from Aldrich) was distilled under vacuum prior to use. Ammonium persulfate, perchloric acid, $CuSO_4$, NaCl and $FeSO_4$ were from Merck with p.a. quality and the water employed for the preparation of the solutions was obtained from an Elga Labwater Purelab Ultra system. A natural montmorillonite obtained from Tlemcen (Algeria) was used.

### 2.2 Preparation of Metal Ion-Exchanged Montmorillonites

10 g of natural montmorillonite (M) was suspended in 500 mL of doubly distilled water and stirred using a magnetic stirrer for 48 h. The suspension was centrifuged at 2,000 rpm, and the clear supernatant was decanted. The resultant slurry was dispersed in 500 mL of water and the above procedure was repeated until the supernatant was free of any impurities. This procedure removed most of the organic impurities present in the clay along with some of the fine clay particles. The dry mass of the final clay was around 5 g. The slurry thus obtained was stirred for 24 h with either 100 mL of 1 M NaCl (aq) or 1 M $CuSO_4$ (aq) or 1 M $FeSO_4$ (aq) solution to exchange cations present in the clay for $Na^+$, $Cu^{2+}$ or $Fe^{2+}$. The resultant colloid was centrifuged and the supernatant discarded. The slurry thus obtained was then stirred with distilled water and, as before, the suspension was centrifuged and the supernatant was discarded. This procedure was repeated until the supernatant [tested using $AgNO_3$ (aq)] was free of $Cl^-$ ions. The slurry thus obtained is the M containing hydrated $Na^+$ (Na-M), hydrated $Cu^{2+}$ (Cu-M) or hydrated $Fe^{2+}$ ions (Fe-M) within the interlayer spaces. The products were dried at 383 K, overnight and its composition was measured by X-ray fluorescence, obtaining the data in Table 1.

### 2.3 Preparation of PANI/Montmorillonite Nanocomposites

The nanocomposites were prepared by the intercalation of aniline in the modified montmorillonite (1 g of Na-M, Cu-M or Fe-M), using an aniline solution and subsequent polymerization as described previously [26, 27]. Briefly, the modified-montmorillonite (Na-M, Cu-M or Fe-M) was dispersed in 100 mL of deionized water using ultrasonication for 5 h. Then, 0.22 mol of aniline was added, followed by the addition of 1 M perchloric acid $HClO_4$. The mixture was stirred for 24 h until the monomer was intercalated into the montmorillonite.

Then, 0.1 M ammonium persulfate solution (dissolved in 1 M aqueous $HClO_4$) was added drop wise, and the mixture was stirred for 24 h at room temperature. The obtained precipitate of the nanocomposites was filtered, and washed several times with deionized water and methanol to remove unreacted monomers and $HClO_4$. The samples were dried under vacuum at 333 K for 24 h.

### 2.4 Nanocomposites Characterization

The XRD of the powder nanocomposites were taken using a Bruker CCD-Apex equipment with a X-ray generator (Cu K$\alpha$ and Ni filter) operated at 40 kV and 40 mA. X-ray fluorescence spectroscopy of the powder nanocomposites was made using a Philips PW1480 equipment with a UNIQUANT II software to determine elements in a semi quantitative way.

For recording the UV–Vis absorption spectra, a Hitachi U-3000 spectrophotometer was used. The solution of the polymer in *N*-methyl-2-pyrrolidone (NMP) was used for recording the spectrum. FTIR was recorded using a Bruker Alpha spectrometer. For TEM observations, the samples were dried under vacuum and supported on TEM grids.

**Table 1** Elemental composition (wt%) of modified-montmorillonites (Na-M, Cu-M and Fe-M) and raw montmorillonite (M)

| Composition (wt%) | $SiO_2$ | $Al_2O_3$ | $Fe_2O_3$ | CaO | $Na_2O$ | $ZrO_2$ | MgO | $K_2O$ | $TiO_2$ | $Cl^-$ | CuO |
|---|---|---|---|---|---|---|---|---|---|---|---|
| M | 71.97 | 16.86 | 2.45 | 0.08 | 0.97 | 0.06 | 3.38 | 2.88 | 0.55 | 0.89 | – |
| Na-M | 73.40 | 17.72 | 1.95 | 0.01 | 2.66 | 0.01 | 2.60 | 1.48 | 0.17 | – | – |
| Cu-M | 74.45 | 16.35 | 2.06 | 0.01 | – | 0.01 | 1.80 | 1.63 | 0.35 | – | 3.34 |
| Fe-M | 72.81 | 17.35 | 5.43 | 0.01 | – | 0.01 | 2.75 | 1.48 | 0.16 | – | – |

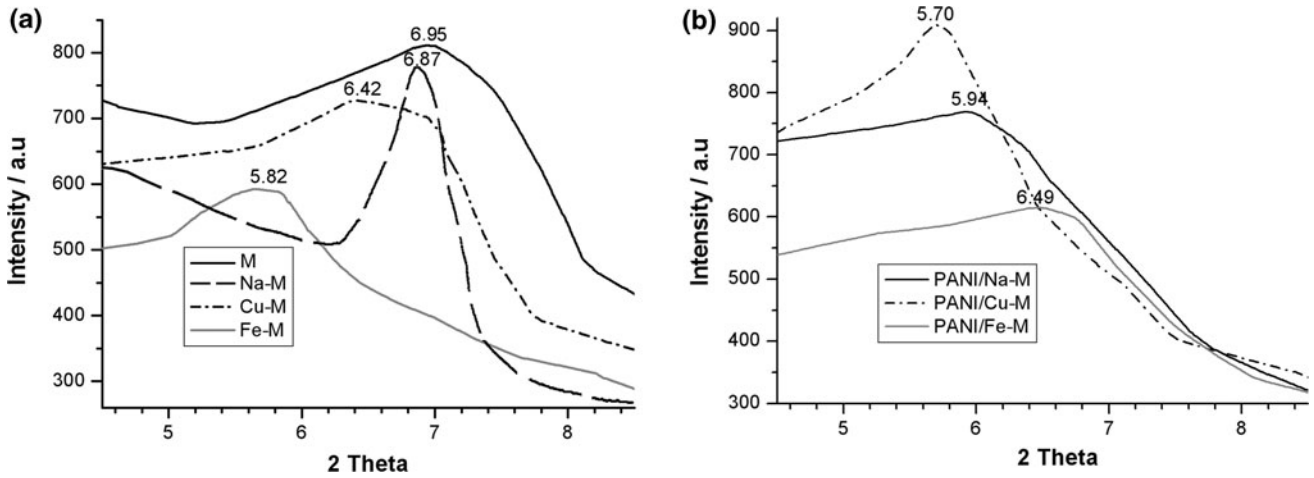


**Fig. 1** XRD diffraction patterns of **a** the montmorillonites (M, Na-M, Cu-M and Fe-M); **b** the nanocomposites (PANI/Na-M, PANI/Cu-M and PANI/Fe-M)

The images were collected using a JEOL (JEM-2010) microscope, working at an operation voltage of 200 kV.

### 2.5 Electrochemical Characterization

The electrochemical behaviour of the polymers was studied by cyclic voltammetry after their extraction from the montmorillonite by dissolving in NMP. It is known that this kind of conducting polymers are soluble in NMP [28], while the clay remains in solid state. Thus, both components can be separated by filtration. The electrochemical measurements were carried out using a conventional three electrodes cell. The counter and reference electrodes were a platinum foil and a reversible hydrogen electrode, respectively. The polymer films were obtained by casting a drop of the NMP polymer solution over the working graphite electrode and heating with an infrared lamp to remove the solvent. The electrolyte used was 1 M $HClO_4$ and all experiments were carried out at 50 mV $s^{-1}$.

### 2.6 Electrical Conductivity Measurements

Electrical conductivity measurements were carried out using a Lucas Lab resistivity equipment with four probes in-line. The samples were dried in vacuum during 24 h and pellets of 0.013 m diameter were prepared using a FTIR mold by applying a pressure of 7.4 $10^8$ Pa.

## 3 Results and Discussion

### 3.1 XRD Characterization

The Na-M, Cu-M and Fe-M modified clays and the raw montmorillonite were characterized using XRD to check changes in the interlayer spacing (Fig. 1a). The XRD patterns show that the (001) diffraction peak between 5.5° and 6.5°, changes depending on the inorganic cation intercalated. Table 2 includes the *d*-spacing between the montmorillonite sheets calculated from the Bragg equation ($n\lambda = 2d\ \sin\theta$, $\lambda = 1.5418$ Å Cu K$\alpha$1) [29], the ionic radii, the solvated radii (i.e., stokes radii) and the maximum $2\theta$ values of the peaks. This table shows that the size of the solvated cation rather than the ionic size determines the layer expansion [30].

The diffraction patterns of PANI/Na-M, PANI/Cu-M and PANI/Fe-M nanocomposites are shown in Fig. 1b. Table 3 summarizes the XRD data obtained for the nanocomposites. Although the diffraction patterns are similar for PANI/Na-M and PANI/Fe-M samples, the (001) diffraction peak for PANI/Cu-M has a more pronounced peak at lower angles

**Table 2** Ionic radii, stokes radii, peak maximum and *d*-spacing of different inorganic cations intercalated in montmorillonite

| Ion | Ionic radii (Å) | Stokes radii (Å) | $2\theta_{max}$ peak máximum | Basal spacing $d_{(001)}$ (Å) |
|---|---|---|---|---|
| $Na^+$ | 1.02 | 1.63 | 6.97 | 12.66 |
| $Cu^{2+}$ | 0.73 | 5.79 | 6.42 | 13.75 |
| $Fe^{2+}$ | 0.82 | 2.81 | 5.82 | 15.16 |

**Table 3** Peak maximum and *d*-spacing of the PANI/clay nanocomposites

| Samples | PANI/Na-M | PANI/Cu-M | PANI/Fe-M |
|---|---|---|---|
| Peak maximum, $2\theta$ max (deg) | 5.94 | 5.70 | 6.49 |
| Basal spacing, $d_{(001)}$ (Å) | 14.86 | 15.48 | 13.60 |

($2\theta = 5.70°$). PANI/Na-M nanocomposite has a basal spacing of 14.86 Å (which is higher than that for Na-M, Table 2) and this parameter is 15.48 Å for PANI/Cu-M sample which is also higher than the value obtained for Cu-M, suggesting the intercalation of PANI between the layers. The shoulder found in PANI/Cu-M at lower angles, suggests the existence of different conformations of the intercalated species. Yoshimoto et al. [31, 32] observed a similar change in the diffraction peak when they intercalated different amounts of anilinium salts into montmorillonite layers. These authors attributed this change to the existence of two types of conformations of intercalated species depending on the anilinium concentration [31]. Thus, in a similar way, the PANI/Cu-M sample can lead to different structures with different basal spacings.

The intercalation of $Fe^{2+}$ and PANI into the M layers has been observed by XRD patterns. XRD pattern of Fe-M (Fig. 1a) shows a shift in the peak position to lower 2θ values (5.82°), which means that the basal spacing increases due to $Fe^{2+}$ intercalation to 15.16 Å, what confirms the modification of the clay [33]. However, *d*-spacing value decreases after the intercalation of PANI into the Fe-M layers from 15.16 to 13.60 Å (Tables 2, 3), what is due to the exfoliation of montmorillonite by the polymer.

### 3.2 FTIR Spectroscopy

The FTIR spectra of modified montmorillonites (Na-M, Cu-M, Fe-M) and PANI/clay nanocomposites (PANI/Na-M, PANI/Cu-M, PANI/Fe-M) are shown in Fig. 2. The spectra of Na-M, Cu-M and Fe-M show the characteristic bands of silicate montmorillonite. These bands can be assigned as follows: the band at around 3,623 $cm^{-1}$ is due to O–H stretching vibration, the one at 1,626 $cm^{-1}$ is due to H–O–H bending, the one at 1,007 $cm^{-1}$ can be associated to Si–O stretching, the bands at 919 and 787 $cm^{-1}$ are due to Al–O stretching and the one at 515 $cm^{-1}$ is due to Si–O–Al stretching vibration [34].

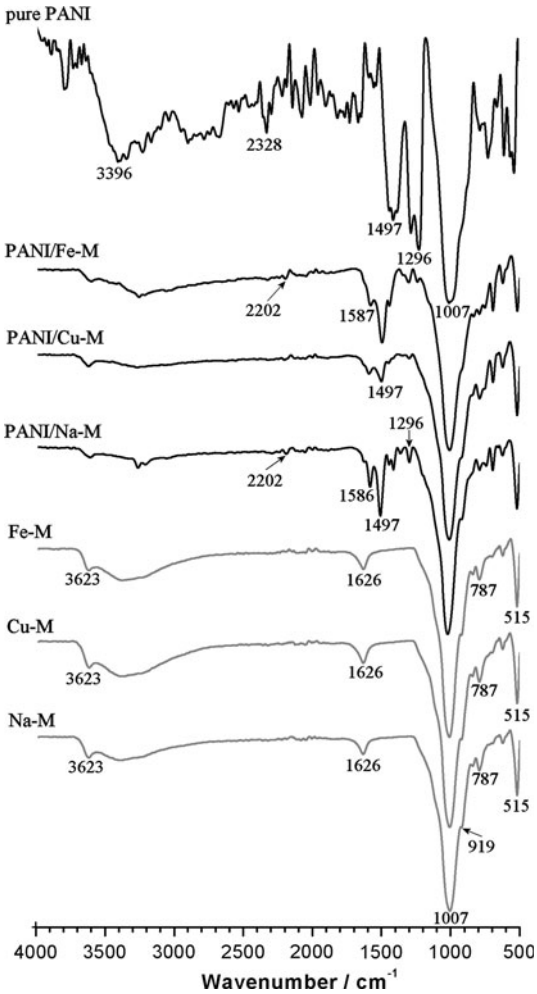


**Fig. 2** FTIR spectra of Na-M, Cu-M, Fe-M, PANI/Na-M, PANI/Cu-M, PANI/Fe-M and pure PANI

The presence of PANI inside interlayer spaces of modified-montmorillonites results in the enhancement of the intensity of the 3,200–3,500 $cm^{-1}$ band along with a decrease of intensity of the bands due to Si–O and Al–O vibrations. The increase in intensity of the 3,200–3,500 $cm^{-1}$ band reflects the hydrogen bonding between the hydroxyl species and $NH_3^+$ group of the PANI. Likewise, the decrease in the intensity of the Si–O, Al–O, and Si–O–Al bands in presence of anilinium ions could be explained considering that when the protons in anilinium ions are hydrogen-bonded to the oxygen species of Si–O, Al–O, and Si–O–Al of the montmorillonite, these bonds will weaken and the tetrahedral symmetry of these moieties in the clay will be distorted. This would result in the change of the IR band positions as well as in the decrease in the intensities of the bands.

**Table 4** The electrical conductivity values of modified montmorillonites and PANI/clay nanocomposites

| Samples | Na-M | Cu-M | Fe-M | PANI/Na-M | PANI/Cu-M | PANI/Fe-M |
|---|---|---|---|---|---|---|
| Conductivity ($10^{-5}$ S cm$^{-1}$) | 1.74 | 4.51 | 0.96 | 12.76 | 24.19 | 15.45 |

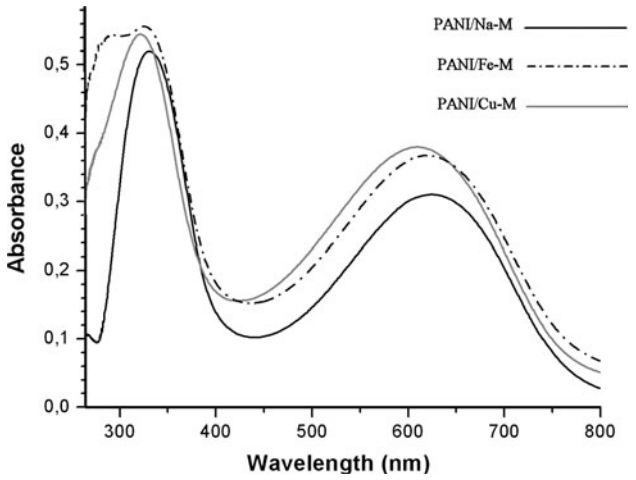


**Fig. 3** UV-vis spectra of the PANI/Na-M, PANI/Cu-M and PANI/Fe-M nanocomposites

**Table 5** Position of the UV–Vis absorption bands of PANI/Na-M, PANI/Cu-M and PANI/Fe-M nanocomposites

| Nanocomposites | PANI/Na-M | PANI/Cu-M | PANI/Fe-M |
|---|---|---|---|
| Band gap ($\lambda_{max}$ nm) | 329 | 322 | 289–330 |
| Exciton ($\lambda_{max}$ nm) | 625 | 611 | 622 |

The appearance of additional bands at around 1,497, 1,296 cm$^{-1}$ and the shifts of the band positions are attributable to the amine group. The bands at 1,586 and 1,497 cm$^{-1}$ have been assigned for benzenoid N–B–N and quinoid N=Q=N vibrations where B stands for benzenoid segments in PANI and Q for quinoid segments [35–37].

### 3.3 Electrical Conductivity Characterization

Table 4 shows the electrical conductivities of modified-montmorillonites. It can be observed an increase in the conductivity with the cation exchange, decreasing in the order Cu-M > Na-M > Fe-M. The presence of the polymer improves the electronic conductivity. The values of conductivity of the PANI/clay nanocomposites lie between 24.19 × $10^{-5}$ and 12.76 × $10^{-5}$ S cm$^{-1}$ being the nanocomposite with copper the one that shows the higher conductivity.

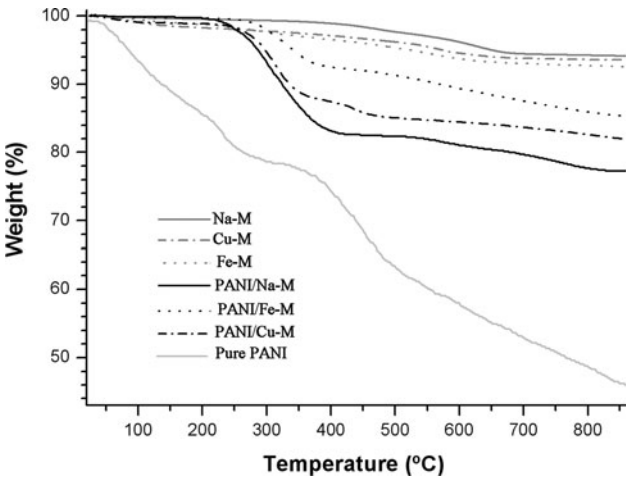


**Fig. 4** Thermogravimetric curves of Na-M, Cu-M, Fe-M, PANI/Na-M, PANI/Cu-M, PANI/Fe-M and pure PANI obtained in $N_2$ atmosphere at heating rate of 10 °C min$^{-1}$

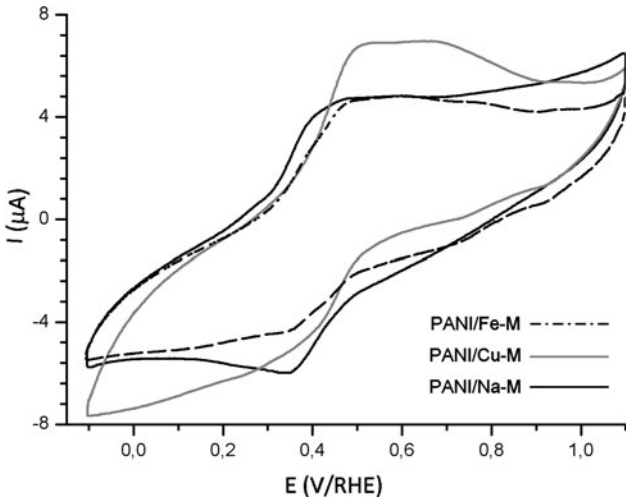


**Fig. 5** Cyclic voltammograms recorded for a graphite electrode covered by PANI/Na-M, PANI/Cu-M and PANI/Fe-M nanocomposites in 1 M $HClO_4$ solution. Scan rate 50 mV/s

The electrical conductivity of PANI/Fe-M was slightly increased with respect to PANI/Na-M sample. This may be attributed to the intercalation of the PANI chains between the Na-M layers which cause the formation of short conducting polymer chains. The contrary behavior was reported for the PANI/Fe-M that formed an exfoliated nanocomposite.

### 3.4 UV–Vis Spectroscopy

The UV–Vis spectra of nanocomposites in NMP solution are shown in Fig. 3. The absorption maxima for the nanocomposites are included in Table 5. There are two

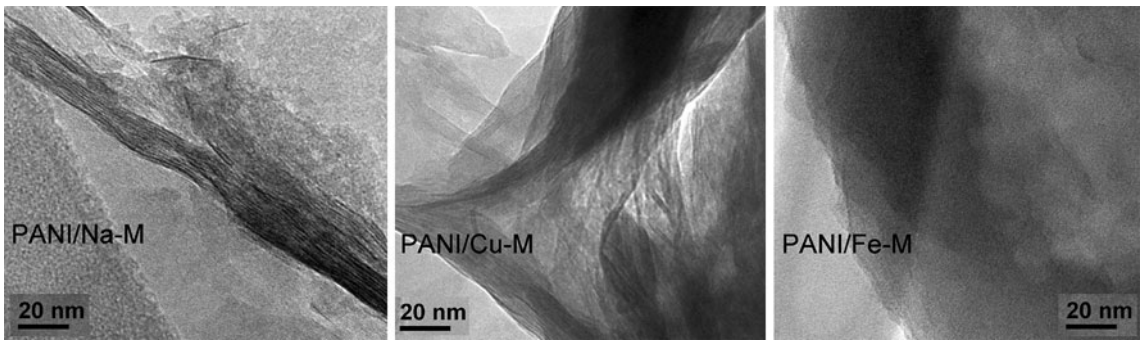


**Fig. 6** TEM images of the PANI/Na-M, PANI/Cu-M and PANI/Fe-M nanocomposites

absorption bands in the electronic spectra of the samples. The first band at around ~350 nm is assigned to π–π* transitions which corresponds to the band gap and the second band at above ~600 nm can be assigned to polaron–π* exciton band or to a charge transfer band associated with the excitation of benzenoid to quinoid rings [38, 39].

### 3.5 Thermogravimetric Analysis (TGA)

To analyze the thermal stability of the PANI/clay nanocomposites, TGA was performed. Figure 4 shows the TGA curves for the Na-M, Cu-M and Fe-M, pure PANI and PANI/clay nanocomposites, measured under a nitrogen atmosphere. The degradation temperatures of the materials were measured from the intersection of the tangents of the initial part and the inflection point of the curve. The experiments for modified montmorillonites (Na-M, Cu-M and Fe-M) contain the typical features for M, a first process at low temperatures (at around 75 °C) which corresponds to the evolution of weakly bonded water molecules and a second one at around 600 °C that corresponds to the dehydroxilation of the octahedral sheet. The PANI/Na-M, PANI/Cu-M and PANI/Fe-M nanocomposites present two degradation stages. The first process occurs at around 100 °C that corresponds to the removal of adsorbed molecules such water and monomers that have not polymerized. The second degradation process occurs at around 250 °C, with a weight loss between 10 and 20 wt% depending on the nanocomposite, that can be assigned to decomposition of the organic polymer [40]. Also, the weight loss for the second stage of decomposition was lower compared to pure PANI decomposition. The nanocomposites particles with a high aspect ratio may hinder the degradation process providing a barrier to preclude evaporation of small molecules generated during the thermal decomposition process. According to Zanetti et al. [41], the barrier effect of the clay increases during volatilization because of the reassembly of the silicate layers on the polymer surface by the thermal decomposition of the polymer present in the nanocomposite. At higher temperatures a continuous weight loss is observed for all the nanocomposites.

### 3.6 Electrochemical Properties

Cyclic voltammetry experiments were performed to test the electroactivity of the PANI extracted from the nanocomposites. Figure 5 shows the steady voltammograms of PANI from PANI/Na-M, PANI/Cu-M and PANI/Fe-M samples, obtained in 1 M $HClO_4$ solution at a scan rate of 50 mV $s^{-1}$. In PANI from PANI/Cu-M nanocomposite, two overlapped redox processes are observed. The first one appears at 0.50/0.39 V, which results in a potential peak separation ($\Delta E_p$) close to 110 mV; the second process is observed at 0.67/0.75 V and gives a $\Delta E_p$ value of 80 mV. The first redox process is due to the oxidation of the benzenoid form of PANI and the second one to the oxidation of the quinoid form of PANI. The voltammetric profiles for PANI from PANI/Na-M and PANI/Fe-M, show one redox process centered at 0.41/0.34 and 0.47/0.34 V, respectively.

### 3.7 Transmission Electron Micrographs (TEM)

The TEM images of PANI/Na-M, PANI/Cu-M and PANI/Fe-M nanocomposites are shown in Fig. 6. The images for PANI/Na-M and PANI/Cu-M samples show the clay layers in which polymer chains are intercalated. The PANI/Fe-M sample shows a mixed nanomorphology with the presence of some exfoliation of the clay.

## 4 Conclusions

A series of PANI/clay nanocomposites were prepared by the intercalation of aniline monomer into the interlayer space of montmorillonite modified with different inorganic cations (Na-M, Cu-M and Fe-M). FTIR spectroscopy evidences electrostatic interactions between the PANI chains and the clay layers. XRD and TEM observations suggest

that PANI is intercalated into the layer of the clay for Cu-M and Na-M samples, and in the case of PANI/Fe-M, exfoliation of the clay is produced. Based on the TGA analysis, the PANI chains in the nanocomposites are more thermally stable than those of pure PANI. The room temperature electrical conductivity of the PANI/clay nanocomposites varies from $12.76 \times 10^{-5}$ to $24.19 \times 10^{-5}$ S cm$^{-1}$ depending on the type of inorganic cation intercalated in the clay. Good electrochemical response was observed for the PANI grown into the montmorillonites (Na-M, Cu-M and Fe-M) in which the cyclic voltammograms show reversible redox processes.

**Acknowledgments** This work was supported by the National Agency for the Development of University Research (ANDRU), the Directorate General of Scientific Research and Technological Development (DGRSDT) of Algeria. Ministerio de Economia y Competitividad and FEDER are also acknowledged (MAT2010-15273). The Generalitat Valenciana is also acknowledged (PROMETEO2013/038).

## References

1. S.P. Liu, C.W. Liang, Int. J. Heat Mass. Transf. **38**, 434 (2011)
2. Y. Kim, J.L. White, J. Appl. Polym. Sci. **96**, 1888 (2005)
3. J.J. Decker, S.N. Chvalun, S. Nazarenko, Polymer **52**, 3943 (2011)
4. H. Akat, M.A. Tasdelen, F.D. Prez, Y. Yagci, Eur. Polym. J. **44**, 1949 (2008)
5. S. Kim, A.M. Palomino, Appl. Clay Sci. **51**, 491 (2011)
6. S. Qutubuddin, X. Fu, Y. Tajuddin, Polymer **42**, 807–814 (2005)
7. G. Ragosta, G. Scarinzi, L. Mascia, Polymer **45**, 2182 (2004)
8. J. Morawiee, A. Pawlak, M. Slouf, Eur. Polym. J. **41**, 1115 (2005)
9. K.M. Lee, C.D. Han, Polymer **44**, 4573 (2003)
10. K.M. Lee, C.D. Han, Macromolecules **36**, 804 (2003)
11. J.W. Gilman, Appl. Clay Sci. **15**, 31 (1999)
12. H.A. Klok, S. Lecommandoux, Adv. Mater. **13**, 1217 (2001)
13. C. Sanchez, G.J. Soler-Illia, A.A. de, F. Ribot, T. Lalot, C.R. Mayer, V. Cabuil. Chem. Mater. **13**, 3061 (2001)
14. T. Changyu, C. Nanxi, Z. Qin, W. Ke, F. Qiang, Z. Xinyuan, Polym. Degrad. Stab. **94**, 124 (2009)
15. L. Dongkyu, C. Kookheon, Polym. Degrad. Stab. **75**, 555 (2002)
16. Y. Furukawa, F. Ueda, Y. Hyodo, I. Harada, T. Nakajima, T. Kawagoe, Macromolecules **21**, 1297 (1998)
17. K.G. Conroy, C.B. Breslin, Electrochim. Acta **48**, 721 (2003)
18. J.E. Mark, *Polymer data handbook* (Oxford University Press, New York, 1999)
19. G.M. Nascimento, V.R.L. Constantino, R. Landers, M.L.A. Temperini, Macromolecules **37**, 9373 (2004)
20. S. Yoshimoto, F. Ohashi, Y. Ohnishi, T. Nonami, Synth. Met. **145**, 265 (2004)
21. M. Kaneko, H. Nakamura, J. Chem. Soc. Chem. Commun. **2**, 346 (1985)
22. D. Lee, K. Char, Polym. Degrad. Stab. **75**, 555 (2002)
23. H. Kuhn, R. Gregory, W. Kimbrell, *Int. SAMPE Electron. Conf.*, vol. 3 (1989), p. 570
24. H. Nishino, G. Yu, A.J. Heeger, T.A. Chen, R.D. Rieke, Synth. Met. **68**, 243 (1995)
25. I.D. Parker, J. Appl. Phys. **75**, 1656 (1994)
26. K. Samrana, A. Shahzada, P. Jiri, P. Josef, M.J. Yogesh, J. Mater. Sci. **47**, 420 (2012)
27. Q. Wu, Z. Xue, Z. Qi, F. Wang, Polymer **41**, 2029 (2000)
28. J.H. Sung, H.J. Choi, J. Macromol. Sci. B **44**, 573 (2005)
29. D. Lee, S.H. Lee, K. Char, J. Kim, Macromol. Rapid. Commun. **21**, 1136 (2000)
30. F.C. Huang, F.J. Lee, C.K. Lee, H.P. Chao, Coll. Surf. A **239**, 41 (2004)
31. S. Yoshimoto, F. Ohashi, T. Kameyama, Macromol. Rapid. Commun. **25**, 1687 (2004)
32. I. Toumi, A. Benyoucef, A. Yahiaoui, C. Quijada, E. Morallon, J. Alloy. Compd. **551**, 212 (2013)
33. D. Lee, K. Char, S.W. Lee, Y.W. Park, J. Mater. Chem. **13**, 2942 (2003)
34. R.E. Grim, *Clay Mineralogy,* 2nd edn. (McGraw-Hill, New York, 1968), p. 261
35. R. Murugeshan, E. Subramanian, Mater. Chem. Phys. **77**, 860 (2002)
36. S. Sharma, C. Nirkhe, S. Pethkar, A.A. Aathaawale, Sensor. Actuat. B **85**, 131 (2002)
37. M.J. Wilson, *Infrared Methods* (Chapman and Hall, London, 1994)
38. K. Samrana, A. Shahzada, P. Jiri, P. Josef, M.J. Yogesh, J. Mater. Sci. **47**, 420 (2012)
39. O. Yang, Y. Zhang, H. Li, Y. Zhang, M. Liu, J. Luo, L. Tan, H. Tang, S. Yao, Talanta **81**, 664 (2010)
40. M.A. Soto-Oviedo, O.A. Araujo, R. Faez, M.C. Rezende, M.A. DePaoli, Synth. Met. **156**, 1249 (2006)
41. M. Zanetti, T. Kashiwagi, L. Falqui, G. Camino, Chem. Mater. **14**, 881 (2002)